

Transactions on Networks and Communications

ISSN: 2054-7420

TABLE OF CONTENTS

EDITORIAL ADVISORY BOARD	I
DISCLAIMER	II
A Block Diagram of Electromagnetoelastic Actuator Nanodisplacement for Communications Systems Sergey Mikhailovich Afonin	1
Research of Space Network Node Route Planning and Localization in HAPS Space Hengyang Liu, Xiaoyang Liu, Chao Liu	10
Ecological Methods of Assessing the Quality of the Environment in the Fluctuating Asymmetry of Birch Leaves P.M. Mazurkin	19

Editor In Chief

Dr Patrick J Davies
Ulster University, United Kingdom

EDITORIAL ADVISORY BOARD

- | | |
|---|--|
| Professor Simon X. Yang
The University of Guelph
<i>Canada</i> | Dr Youlian Pan
Information and Communications Technologies
National Research Council <i>Canada</i> |
| Professor Shahram Latifi
Dept. of Electrical & Computer Engineering University of
Nevada, Las Vegas
<i>United States</i> | Dr Xuewen Lu
Dept. of Mathematics and Statistics
University of Calgary
<i>Canada</i> |
| Professor Farouk Yalaoui
University of Technology of Troyes
<i>France</i> | Dr Sabine Coquillart
Laboratory of Informatics of Grenoble
<i>France</i> |
| Professor Julia Johnson
Laurentian University, Sudbury, Ontario
<i>Canada</i> | Dr Claude Godart
University of Lorraine
<i>France</i> |
| Professor Hong Zhou
Naval Postgraduate School Monterey, California
<i>United States</i> | Dr Paul Lukowicz
German Research Centre for Artificial Intelligence
<i>Germany</i> |
| Professor Boris Verkhovsky
New Jersey Institute of Technology, New Jersey
<i>United States</i> | Dr Andriani Daskalaki
Max Planck Institute for Molecular Genetics
MOLGEN
<i>Germany</i> |
| Professor Jai N Singh
Barry University, Miami Shores, Florida
<i>United States</i> | Dr Jianyi Lin
Department of Computer Science
University of Milan, <i>Italy</i> |
| Professor Don Liu
Louisiana Tech University, Ruston
<i>United States</i> | Dr Hiroyuki SATO
Information Technology Centre
The University of Tokyo
<i>Japan</i> |
| Dr Steve S. H. Ling
University of Technology, Sydney
<i>Australia</i> | Dr Christian Cachin
IBM Research – Zurich
<i>Switzerland</i> |
| Dr Yuriy Polyakov
New Jersey Institute of Technology, Newark
<i>United States</i> | Dr W. D. Patterson
School of Computing, Ulster University
<i>United Kingdom</i> |
| Dr Lei Cao
Department of Electrical Engineering, University of
Mississippi
<i>United States</i> | Dr Alia I. Abdelmoty
Cardiff University, Wales
<i>United Kingdom</i> |
| Dr Kalina Bontcheva
Dept. of Computer Science
University of Sheffield, <i>United Kingdom</i> | Dr Sebastien Lahaie
Market Algorithms Group, Google
<i>United States</i> |
| Dr Bruce J. MacLennan
University of Tennessee, Knoxville, Tennessee
<i>United States</i> | Dr Jenn Wortman Vaughan
Microsoft
<i>United States</i> |
| Dr Panayiotis G. Georgiou
USC university of Southern California, Los Angeles
<i>United States</i> | Dr Jianfeng Gao
Microsoft
<i>United States</i> |
| Dr Armando Bennet Barreto
Dept. Of Electrical and Computer Engineering
Florida International University
<i>United States</i> | Dr Silviu-Petru Cucerzan
Machine Learning Department, Microsoft
<i>United States</i> |
| Dr Christine Lisetti
School of Computing and Information Sciences | Dr Ofer Dekel
Machine Learning and Optimization Group, Microsoft
<i>Israel</i> |
-

Florida International University
United States

Dr K. Ty Bae
Department of Radiology
University of Pittsburgh
United States

Dr Jiang Hsieh
Illinois Institute of Technology
University of Wisconsin-Madison
United States

Dr David Bulger
Department of Statistics
MACQUARIE University
Australia

Dr YanXia Lin
School of Mathematics and Applied Statistics
University of Wollongong
Australia

Dr Marek Reformat
Department of Electrical and Computer Engineering
University of Alberta
Canada

Dr Wilson Wang
Department of Mechanical Engineering
Lake head University
Canada

Dr Joel Ratsaby
Department of Electrical Engineering and Electronics
Ariel University
Israel

Dr Naoyuki Kubota
Department of Mechanical EngineeringTokyo
Metropolitan University
Japan

Dr Kazuo Iwama
Department of Electrical Engineering
Koyoto University
Japan

Dr Stefanka Chukova
School of Mathematics and Statistics
Victoria University of Wellington
New Zealand

Dr Ning Xiong
Department of Intelligent Future Technologies
Malardalen University
Sweden

Dr Khosrow Moshirvaziri
Department of Information systems
California State University Long Beach
United States

Dr Kechen Zhang
Department of Biomedical Engineering
Johns Hopkins University
United States

Dr. Jun Xu
Sun Yat-Sen University , Guangzhou
China

Dr Dinie Florancio
Multimedia Interaction and Collaboration Group
Microsoft
United States

Dr Jay Stokes
Department of Security and Privacy, Microsoft
United States

Dr Tom Burr
Computer, Computational, and Statistical Sciences Division
Los Alamos National Laboratory
United States

Dr Philip S. Yu
Department of Computer Science
University of Illinois at Chicago
United States

Dr David B. Leake
Department of Computer Science
Indiana University
United States

Dr Hengda Cheng
Department of Computer Science
Utah State University
United States

Dr. Steve Sai Ho Ling
Department of Biomedical Engineering
University of Technology Sydney
Australia

Dr. Igor I. Baskin
Lomonosov Moscow State University,
Moscow
Russian Federation

Dr. Konstantinos Blekas
Department of Computer Science & Engineering,
University of Ioannina
Greece

Dr. Valentina Dagiene
Vilnius University
Lithuania

Dr. Francisco Javier Falcone Lanas
Department of Electrical Engineering,
Universidad Publica de Navarra, UPNA
Spain

Dr. Feng Lin
School of Computer Engineering
Nanyang Technological University
Singapore

Dr. Remo Pareschi
Department of Bioscience and Territory
University of Molise
Italy

Dr. Hans-Jörg Schulz
Department of Computer Science
University of Rostock
Germany

Dr. Alexandre Varnek
University of Strasbourg
France

DISCLAIMER

All the contributions are published in good faith and intentions to promote and encourage research activities around the globe. The contributions are property of their respective authors/owners and the journal is not responsible for any content that hurts someone's views or feelings etc.

A Block Diagram of Electromagnetoelastic Actuator Nanodisplacement for Communications Systems

Sergey Mikhailovich Afonin

National Research University of Electronic Technology (MIET), Moscow, Russia;
eduems@mail.ru

ABSTRACT

The parametric block diagram of the electromagnetoelastic actuator nanodisplacement or the piezoactuator is determined in contrast the electrical equivalent circuit types Cady or Mason for the calculation of the piezoelectric transmitter and receiver, the vibration piezomotor with the mechanical parameters in form the velocity and the pressure. The method of mathematical physics is used. The parametric block diagram of electromagnetoelastic actuator is obtained with the mechanical parameters the displacement and the force. The transfer functions of the electroelastic actuator are determined. The the generalized parametric block diagram, the generalized matrix equation for the electromagnetoelastic actuator nanodisplacement are obtained. The deformations of the electroelastic actuator for the nanotechnology are described by the matrix equation. Block diagram and structural-parametric model of electromagnetoelastic actuator nanodisplacement for nanodisplacement of the communications systems are obtained, its transfer functions are built. Effects of geometric and physical parameters of electromagnetoelastic actuators and external load on its dynamic characteristics are determined. For calculations the communications systems with the piezoactuator for nanodisplacement the parametric block diagram and the transfer functions of the piezoactuator are obtained.

Keywords: Electromagnetoelastic actuator; Parametric block diagram; Matrix transfer function; Piezoactuator.

1 Introduction

The parametric block diagram of electromagnetoelastic actuator for nanodisplacement on the piezoelectric, piezomagnetic, electrostriction, magnetostriction effects, for example, the piezoactuator is determined in contrast electrical equivalent circuit types Cady or Mason for the calculation of the piezotransmitter and piezoreceiver, the vibration piezomotor with the mechanical parameters in form the velocity and the pressure [1 – 11]. The block diagram of electromagnetoelastic actuator is obtained with the mechanical parameters the displacement and the force [7 - 9]. The electromagnetoelastic actuator is used for precise alignment in the nanotechnology, the adaptive optics, the communications systems. The piezoactuator of nanometric movements operates based on the inverse piezoeffect, in which the motion is achieved due to deformation of the piezoactuator when an external electric voltage is applied to it [1 – 19].

Piezoactuator - piezomechanical device intended for actuation of mechanisms, systems or management based on the piezoelectric effect, converts the electrical signals into the mechanical movement or the

force [13 – 15]. The piezoactuators for the drives of nano- and micrometric movements provide the movement range from several nanometers to tens of microns, the sensitivity of up to 10 nm/V, the loading capacity of up to 1000 N, and the transmission band of up to 100 Hz. The investigation of the static and dynamic characteristics of the piezoactuator is necessary for the calculation mechatronics systems of the nano- and micrometric movements for the communications systems. The piezoactuators provide high stress and speed of operation and return to the initial state when switched off; they have very low displacements. The piezoactuators are used in the majority of nanomanipulators for scanning tunneling microscopes, scanning force microscopes, and atomic force microscopes. The nanorobotic manipulators of nano- and microdisplacements with the piezoactuators are the key component in nanorobotic systems. The main requirement for nanomanipulators is to guarantee the positioning accurate to nanometers.

By solving the wave equation with allowance for the corresponding equation of the electromagnetoelasticity, the boundary conditions on loaded working surfaces of the electromagnetoelastic actuators, and the strains along the coordinate axes, it is possible to construct the structural parametric model of the actuator [8, 9, 18]. The transfer functions and the parametric block diagrams of the electromagnetoelastic actuators are obtained from the set of equations describing the corresponding structural parametric model of the actuator for the communications systems. The method of mathematical physics is applied for the solution of the wave equation of the electromagnetoelastic actuator for the communications systems with using the Laplace transform for the construction the parametric block diagram of the electromagnetoelastic actuator. As the result of the joint solution of the wave equation of the actuator with the Laplace transform, the equation of the electromagnetoelasticity, the boundary conditions on the two loaded working surfaces of the actuator, we obtain the corresponding structural-parametric model and the parametric block diagram of the electromagnetoelastic actuator.

2 Block Diagram of Electromagnetoelastic Actuator

The parametric block diagram and the matrix transfer functions of the electromagnetoelastic actuator for the nanotechnology are obtained from the structural-parametric model of the electromagnetoelastic actuator with the mechanical parameters the displacement and the force. The parametric block diagrams of the voltage-controlled or current-controlled piezoactuator are determined from the generalized structural-parametric model of the electromagnetoelastic actuator.

The equation of the electromagnetoelasticity of the actuator [7, 8, 11] has the form

$$S_i = s_{ij}^{E,H} T_j + d_{mi}^H E_m + d_{mi}^E H_m \quad (1)$$

where S_i is the relative deformation along the axis i , E is the electric field strength, H is the magnetic field strength, $s_{ij}^{E,H}$ is the elastic compliance for $E = \text{const}$, $H = \text{const}$, T_j is the mechanical stress along the axis j , d_{mi}^H is the piezomodule, i.e., the partial derivative of the relative deformation with respect to the electric field strength for constant magnetic field strength, i.e., for $H = \text{const}$, E_m is the electric field strength along the axis m , d_{mi}^E is the magnetostriction coefficient, H_m is the magnetic field strength along the axis m , $i = 1, 2, \dots, 6$, $j = 1, 2, \dots, 6$, $m = 1, 2, 3$.

Let us consider separately effect the electric field strength and the magnetic field strength, therefore the generalized equation of the electromagnetoelasticity has the form

$$S_i = d_{mi} \Psi_m(t) + s_{ij}^{\Psi} T_j(x, t) \quad (2)$$

where $S_i = \partial \xi(x, t) / \partial x$ is the relative displacement along axis i of the cross section of the piezoactuator, $\Psi_m = \{E_m, D_m, H_m\}$ is the control parameter E_m for the voltage control, D_m for the current control, H_m for magnetic field strength control along axis m , T_j is the mechanical stress along axis j , d_{mi} is the coefficient of electromagnetoelasticity, for example, piezomodule, s_{ij}^{Ψ} is the elastic compliance for the control parameter $\Psi = \text{const}$.

The main size is determined us the working length $l = \{\delta, h, b\}$ for the actuator or the piezoactuator in form the thickness, the height and the width for the longitudinal, transverse and shift the piezoeffect.

For the construction the parametric block diagram of the electromagnetoelastic actuator in nanotechnology is used the wave equation for the wave propagation in a long line with damping but without distortions. With using Laplace transform is obtained the linear ordinary second-order differential equation with the parameter s . Correspondingly the original problem for the partial differential equation of hyperbolic type using the Laplace transform is reduced to the simpler problem [8, 14, 18] for the linear ordinary differential equation

$$d^2 \Xi(x, s) / dx^2 - \gamma^2 \Xi(x, s) = 0 \quad (3)$$

with its solution

$$\Xi(x, s) = C e^{-\gamma x} + B e^{\gamma x} \quad (4)$$

where $\Xi(x, s)$ is the Laplace transform of the displacement of section of the actuator, $\gamma = s/c^{\Psi} + \alpha$ is the propagation coefficient, c^{Ψ} is the sound speed for $\Psi = \text{const}$, α is the damping coefficient, C and B are constants.

From generalized electromagnetoelasticity equation (3), we obtain the system of equations describing the generalized structural-parametric model of the electromagnetoelastic actuator for the communications systems:

$$\begin{aligned} \Xi_1(s) &= [1/(M_1 s^2)] \times \\ &\times \left\{ -F_1(s) + (1/\chi_{ij}^{\Psi}) [v_{mi} \Psi_m(s) - [\gamma / \text{sh}(l\gamma)] [\text{ch}(l\gamma) \Xi_1(s) - \Xi_2(s)]] \right\} \\ \Xi_2(s) &= [1/(M_2 s^2)] \times \\ &\times \left\{ -F_2(s) + (1/\chi_{ij}^{\Psi}) [v_{mi} \Psi_m(s) - [\gamma / \text{sh}(l\gamma)] [\text{ch}(l\gamma) \Xi_2(s) - \Xi_1(s)]] \right\} \end{aligned} \quad (5)$$

$$\text{where } v_{mi} = \begin{cases} d_{33}, d_{31}, d_{15} \\ g_{33}, g_{31}, g_{15} \\ d_{33}, d_{31}, d_{15} \end{cases}, \Psi_m = \begin{cases} E_3, E_1 \\ D_3, D_1 \\ H_3, H_1 \end{cases}, s_{ij}^{\Psi} = \begin{cases} s_{33}^E, s_{11}^E, s_{55}^E \\ s_{33}^D, s_{11}^D, s_{55}^D \\ s_{33}^H, s_{11}^H, s_{55}^H \end{cases}, c^{\Psi} = \begin{cases} c^E \\ c^D \\ c^H \end{cases}, \gamma = \begin{cases} \gamma^E \\ \gamma^D \\ \gamma^H \end{cases}, l = \begin{cases} \delta \\ h \\ b \end{cases}, \chi_{ij}^{\Psi} = s_{ij}^{\Psi} / S_0,$$

then parameters $\Psi_m = \{E_m, D_m, H_m\}$ of the control for the electromagnetoelastic actuator, v_{mi} is the coefficient of the electromagnetoelasticity, for example, d_{mi} is the piezomodule for the voltage-controlled piezoactuator, g_{mi} is the piezomodule for the current-controlled piezoactuator, d_{mi} is the coefficient of the magnetostriction, S_0 is the cross section area and M_1, M_2 are the displaced mass on

the faces of the electromagnetoelastic actuator, $\Xi_1(s)$, $\Xi_2(s)$ and $F_1(s)$, $F_2(s)$ are the Laplace transform of the displacements and the forces on the faces of the electromagnetoelastic actuator. Figure 1 shows the generalized parametric block diagram of the electromagnetoelastic actuator corresponding to the equation (2) of the electromagnetoelasticity and the set of equations (5).

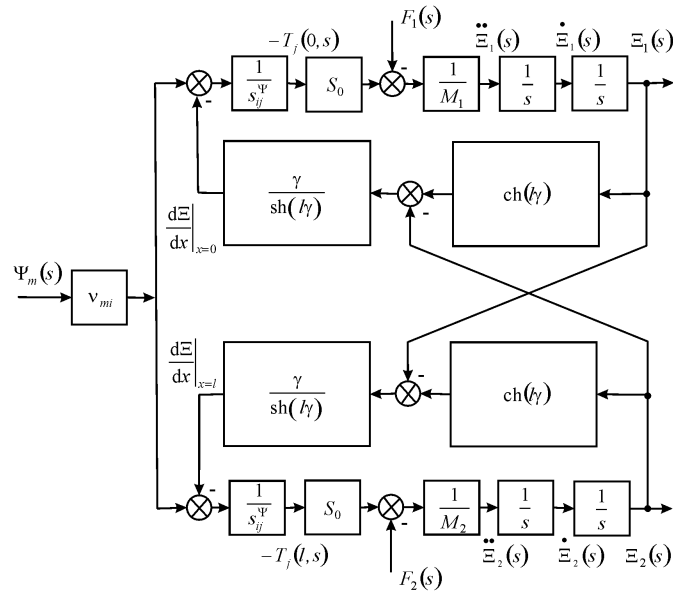


Figure 1. Generalized parametric block diagram of electromagnetoelastic actuator for nanodisplacement

The matrix state equations [11, 14] for the piezoelectric effect have the form

$$(\mathbf{D}) = (\mathbf{d})(\mathbf{T}) + (\boldsymbol{\epsilon}^T)(\mathbf{E}) \quad (6)$$

$$(\mathbf{S}) = (\mathbf{s}^E)(\mathbf{T}) + (\mathbf{d}^Y)(\mathbf{E}) \quad (7)$$

where the equation (6) describes the direct piezoeffect, the equation (7) depicts the inverse piezoeffect, and the matrixes: (\mathbf{D}) is the column-matrix of the electric induction along the coordinate axes, (\mathbf{S}) is the column-matrix of the relative deformations, (\mathbf{T}) is the column-matrix of the mechanical stresses, (\mathbf{E}) is the column-matrix of the electric field strength along the coordinate axes, (\mathbf{d}^Y) is the transposed matrix of the piezoelectric modules, (\mathbf{s}^E) is the elastic compliance matrix, $(\boldsymbol{\epsilon}^T)$ is the matrix of the dielectric constants. In the equation (6), (7) are the six stress components $T_1, T_2, T_3, T_4, T_5, T_6$. The components $T_1 - T_3$ are defined to extension-compression stresses, the components $T_4 - T_6$ are related to shear stresses [8, 11].

Let us consider the transverse piezoelectric effect in the piezoactuator. The equation of the inverse transverse piezoeffect [8, 11]

$$S_1 = d_{31}E_3(t) + s_{11}^E T_1(x, t) \quad (8)$$

where $S_1 = \partial \xi(x, t) / \partial x$ is the relative displacement of the cross section of the piezoactuator along axis 1, d_{31} is the piezoelectric module for the transverse piezoeffect, s_{11}^E is the elastic compliance for $E = \text{const}$ along axis 1, T_1 is the stress along axis 1.

The solution of the linear ordinary second-order differential equation with the parameter s (3) we obtain as (4) and subject to the conditions

$$\begin{aligned}\Xi(0, s) &= \Xi_1(s) \text{ for } x = 0 \\ \Xi(h, s) &= \Xi_2(s) \text{ for } x = h\end{aligned}\quad (9)$$

The constants C and B for the solution are determined in the following form

$$C = (\Xi_1 e^{h\gamma} - \Xi_2) / [2\text{sh}(h\gamma)] \quad , \quad B = (\Xi_2 - \Xi_1 e^{-h\gamma}) / [2\text{sh}(h\gamma)] \quad (10)$$

Then, the solution (4) can be written as

$$\Xi(x, s) = \{\Xi_1(s)\text{sh}[(h-x)\gamma] + \Xi_2(s)\text{sh}(x\gamma)\} / \text{sh}(h\gamma) \quad (11)$$

The equations of forces acting on the faces of the piezoactuator has the form

$$\begin{aligned}T_1(0, s)S_0 &= F_1(s) + M_1 p^2 \Xi_1(s) \text{ for } x = 0 \\ T_1(h, s)S_0 &= -F_2(s) - M_2 s^2 \Xi_2(s) \text{ for } x = h\end{aligned}\quad (12)$$

where $T_1(0, s)$ and $T_1(h, s)$ are determined from the equation of the inverse transverse piezoeffect.

Therefore we obtain the system of the equations for the mechanical stresses at the faces of the piezoactuator for the transverse piezoeffect in the form

$$\begin{aligned}T_1(0, s) &= (1/s_{11}^E) d\Xi(x, s)/dx|_{x=0} - d_{31}E_3(s)/s_{11}^E \\ T_1(h, s) &= (1/s_{11}^E) d\Xi(x, s)/dx|_{x=h} - d_{31}E_3(s)/s_{11}^E\end{aligned}\quad (13)$$

The set of equations (13) for mechanical stresses in piezoactuator yields the following set of equations describing the structural parametric model and the parametric block diagram of the voltage-controlled piezoactuator for the transverse piezoelectric effect on Figure 2

$$\begin{aligned}\Xi_1(s) &= [1/(M_1 s^2)] \times \\ &\times \left\{ -F_1(s) + (1/\chi_{11}^E) [d_{31}E_3(s) - [\gamma/\text{sh}(h\gamma)] [\text{ch}(h\gamma)\Xi_1(s) - \Xi_1(s)]] \right\} \\ \Xi_2(s) &= [1/(M_2 s^2)] \times \\ &\times \left\{ -F_2(s) + (1/\chi_{11}^E) [d_{31}E_3(s) - [\gamma/\text{sh}(h\gamma)] [\text{ch}(h\gamma)\Xi_2(s) - \Xi_1(s)]] \right\}\end{aligned}\quad (14)$$

where $\chi_{11}^E = s_{11}^E/S_0$, $l = h$.

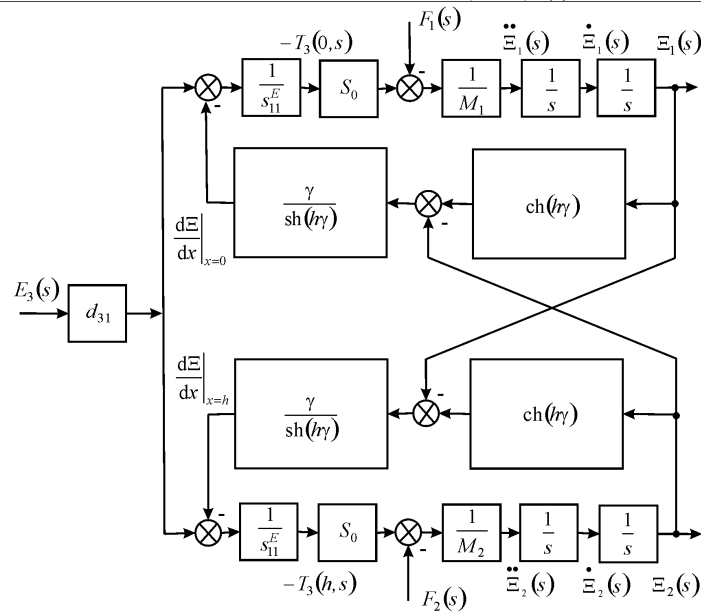


Figure 2. Parametric block diagram of voltage-controlled piezoactuator for transverse piezoeffect

The parametric block diagram of the voltage-controlled or the current-controlled piezoactuator for the transverse, longitudinal, shift piezoelectric effects are determined from the generalized structural-parametric model of the electromagnetoelastic actuator.

3 Matrix transfer function of electromagnetoelastic actuator

From (5), (14) matrix equation of the Laplace transforms of the displacements with the matrix transfer function of the electromagnetoelastic actuator is obtained in the form

$$\begin{aligned}
 (\Xi(s)) &= (W(s))(P(s)) & (15) \\
 (\Xi(s)) &= \begin{pmatrix} \Xi_1(s) \\ \Xi_2(s) \end{pmatrix}, \quad (W(s)) = \begin{pmatrix} W_{11}(s) & W_{12}(s) & W_{13}(s) \\ W_{21}(s) & W_{22}(s) & W_{23}(s) \end{pmatrix} \\
 (P(s)) &= \begin{pmatrix} \Psi_m(s) \\ F_1(s) \\ F_2(s) \end{pmatrix}
 \end{aligned}$$

where $(\Xi(s))$ is the column-matrix of the Laplace transforms of the displacements, $(W(s))$ is the matrix transfer function, $(P(s))$ the column-matrix of the Laplace transforms of the control parameter and the forces.

The generalized transfer functions of the electromagnetoelastic actuator are the ratio of the Laplace transform of the displacement of the face and the Laplace transform of the corresponding control parameter or the force at zero initial conditions

$$\begin{aligned}
 W_{11}(s) &= \Xi_1(s)/\Psi_m(s) = v_{mi} [M_2 \chi_{ij}^\Psi s^2 + \gamma \text{th}(t\gamma/2)] / A_{ij} \\
 \chi_{ij}^\Psi &= s_{ij}^\Psi / S_0
 \end{aligned}$$

$$\begin{aligned}
 A_{ij} &= M_1 M_2 (\chi_{ij}^\Psi)^2 s^4 + \left\{ (M_1 + M_2) \chi_{ij}^\Psi / [c^\Psi \operatorname{th}(l\gamma)] \right\} s^3 + \\
 &+ \left[(M_1 + M_2) \chi_{ij}^\Psi \alpha / \operatorname{th}(l\gamma) + 1 / (c^\Psi)^2 \right] s^2 + 2\alpha s / c^\Psi + \alpha^2 \\
 W_{21}(s) &= \Xi_2(s) / \Psi_m(s) = v_{ij} [M_1 \chi_{ij}^\Psi s^2 + \gamma \operatorname{th}(l\gamma/2)] / A_{ij} \\
 W_{12}(s) &= \Xi_1(s) / F_1(s) = -\chi_{ij}^\Psi [M_2 \chi_{ij}^\Psi s^2 + \gamma / \operatorname{th}(l\gamma)] / A_{ij} \\
 W_{13}(s) &= \Xi_1(s) / F_2(s) = \\
 &= W_{22}(s) = \Xi_2(s) / F_1(s) = [\chi_{ij}^\Psi \gamma / \operatorname{sh}(l\gamma)] / A_{ij} \\
 W_{23}(s) &= \Xi_2(s) / F_2(s) = -\chi_{ij}^\Psi [M_1 \chi_{ij}^\Psi s^2 + \gamma / \operatorname{th}(l\gamma)] / A_{ij}
 \end{aligned}$$

The static displacements of the faces for the voltage-controlled the piezoactuator for the shift piezoeffect are obtained from (15) at $m \ll M_1$ and $m \ll M_2$ in the form

$$\xi_1(\infty) = (M_2 U_0 d_{15} b / \delta) / (M_1 + M_2) \quad (16)$$

$$\xi_2(\infty) = (M_1 U_0 d_{15} b / \delta) / (M_1 + M_2) \quad (17)$$

For the voltage-controlled the piezoactuator from PZT under the shift piezoeffect at $m \ll M_1$ and $m \ll M_2$, $d_{15} = 4 \cdot 10^{-10}$ m/V, $b/\delta = 10$, $U = 50$ V, $M_1 = 1$ kg and $M_2 = 4$ kg the static displacements of the faces the piezoactuator are determined $\xi_1(\infty) = 160$ nm, $\xi_2(\infty) = 40$ nm, $\xi_1(\infty) + \xi_2(\infty) = 200$ nm.

The transfer function of the voltage-controlled transverse piezoactuator is obtained from (14) for elastic-inertial load at $M_1 \rightarrow \infty$, $m \ll M_2$ and the approximation the hyperbolic cotangent by two terms of the power series in the form

$$W(s) = \Xi_2(s) / U(p) = k_t / (T_t^2 s^2 + 2T_t \xi_t s + 1) \quad (18)$$

$$k_t = (d_{31} h / \delta) / (1 + C_e / C_{11}^E), \quad T_t = \sqrt{M_2 / (C_e + C_{11}^E)}, \quad \xi_t = \alpha h^2 C_{11}^E / \left(3c^E \sqrt{M_2 (C_e + C_{11}^E)} \right)$$

where $U(p)$ is the Laplace transform of the voltage, k_t is the value of the coefficient of the displacement for the voltage-controlled piezoactuator, T_t is the time constant and ξ_t is the damping coefficient of the piezoactuator.

For the voltage-controlled transverse piezoactuator at $M_1 \rightarrow \infty$, $m \ll M_2$ and $d_{31} = 2.5 \cdot 10^{-10}$ m/V, $h/\delta = 20$, $M_2 = 1$ kg, $C_{11}^E = 2 \cdot 10^7$ N/m, $C_e = 0.5 \cdot 10^7$ H/m we obtain the value of the coefficient of the displacement and the time constant of the actuator $k_t = 4$ nm/V, $T_t = 0.2 \cdot 10^{-3}$ c.

The matrix transfer function of the actuator is determined for control systems with the electromagnetoelastic actuator in the communications systems.

The generalized parametric block diagram and generalized structural-parametric model of the electromagnetoelastic actuator are obtained. From generalized structural-parametric model of the actuator after algebraic transformations the transfer functions of the actuator are determined.

The parametric block diagram, the structural-parametric models of the piezoactuator for the transverse, longitudinal, shift piezoelectric effects are determined from the generalized structural-parametric model of the electromagnetoelastic actuator for the communications systems.

4 Conclusion

The generalized parametric block diagram and the generalized structural-parametric model of the electromagnetoelastic actuator are constructed with the mechanical parameters the displacement and the force.

The parametric block diagrams of the piezoactuator for the transverse, longitudinal, shift piezoelectric effects are determined. The matrix transfer function of the electromagnetoelastic actuator is obtained for the communications systems.

REFERENCES

- [1] Schultz, J., Ueda, J., Asada, H., *Cellular actuators*. Oxford: Butterworth-Heinemann Publisher, 2017. 382 p.
- [2] Afonin, S.M., *Absolute stability conditions for a system controlling the deformation of an electromagnetoelastic transducer*. Doklady mathematics, 2006. 74(3): p. 943-948, doi:10.1134/S1064562406060391.
- [3] Zhou, S., Yao, Z., *Design and optimization of a modal-independent linear ultrasonic motor*. IEEE transaction on ultrasonics, ferroelectrics, and frequency control, 2014. 61(3): p. 535-546, doi:10.1109/TUFFC.2014.2937.
- [4] Przybylski, J., *Static and dynamic analysis of a flexensional transducer with an axial piezoelectric actuation*. Engineering structures, 2015. 84: p. 140-151, doi:10.1016/j.engstruct.2014.11.025.
- [5] Ueda, J., Secord, T., Asada, H.H., *Large effective-strain piezoelectric actuators using nested cellular architecture with exponential strain amplification mechanisms*. IEEE/ASME transactions on mechatronics, 2010. 15(5): p. 770-782, doi:10.1109/TMECH.2009.2034973.
- [6] Karpelson, M., Wei, G.-Y., Wood, R.J., *Driving high voltage piezoelectric actuators in microrobotic applications*. Sensors and actuators A: Physical, 2012. 176: p. 78-89, doi:10.1016/j.sna.2011.11.035.
- [7] Afonin, S.M., *Block diagrams of a multilayer piezoelectric motor for nano- and microdisplacements based on the transverse piezoeffect*. Journal of computer and systems sciences international, 2015. 54(3): p. 424-439, doi:10.1134/S1064230715020021.
- [8] Afonin, S.M., *Structural parametric model of a piezoelectric nanodisplacement transducer*. Doklady physics, 2008. 53(3) p. 137-143, doi:10.1134/S1028335808030063.
- [9] Afonin, S.M., *Solution of the wave equation for the control of an electromagnetoelastic transducer*. Doklady mathematics, 2006. 73(2), p. 307-313, doi:10.1134/S1064562406020402.
- [10] Cady W.G., *Piezoelectricity: An introduction to the theory and applications of electromechanical phenomena in crystals*. New York, London: McGraw-Hill Book Company, 1946. 806 p.

- [11] *Physical acoustics: Principles and methods. Vol.1. Part A. Methods and devices.* Mason, W., Editor, New York: Academic Press, 1964. 515 p.
- [12] Zwillinger, D., *Handbook of differential equations.* Boston: Academic Press, 1989. 673 p.
- [13] Afonin, S.M., *Structural-parametric model and transfer functions of electroelastic actuator for nano- and microdisplacement.* Chapter 9 in *Piezoelectrics and nanomaterials: Fundamentals, developments and applications.* Parinov, I.A., Editor, New York: Nova Science, 2015. p. 225-242.
- [14] Afonin, S.M., *A structural-parametric model of electroelastic actuator for nano- and microdisplacement of mechatronic system.* Chapter 8 in *Advances in nanotechnology. Volume 19.* Bartul, Z., Trenor, J., Editors, New York: Nova Science, 2017. p. 259-284.
- [15] Afonin, S.M., Nano- and micro-scale piezomotors. *Russian engineering research*, 2012. 32(7-8): p. 519-522, doi:10.3103/S1068798X12060032.
- [16] Afonin, S.M., *Elastic compliances and mechanical and adjusting characteristics of composite piezoelectric transducers.* *Mechanics of solids*, 2007. 42(1): p. 43-49, doi:10.3103/S0025654407010062.
- [17] Afonin, S.M., *Stability of strain control systems of nano-and microdisplacement piezotransducers.* *Mechanics of solids*, 2014. 49(2): p. 196-207, doi:10.3103/S0025654414020095.
- [18] Afonin, S.M., *Structural-parametric model electromagnetoelastic actuator nanodisplacement for mechatronics.* *International journal of physics*, 2017. 5(1): p. 9-15, doi: 10.12691/ijp-5-1-2.
- [19] *Springer Handbook of Nanotechnology.* Bhushan, B., Editor, Springer, Berlin, New York, 2004. 1222 p.

Research of Space Network Node Route Planning and Localization in HAPS Space

¹Hengyang Liu, ^{1,2}Xiaoyang Liu, ¹Chao Liu

¹*School of Computer Science and Engineering, Chongqing University of Technology, Chongqing, 400054, China*

²*College of Engineering, The University of Alabama, Tuscaloosa, Alabama, 35401, USA*
158010342@qq.com; lxy3103@163.com; xiuwenzheng2000@163.com

ABSTRACT

Compared with the traditional method of detection tracking, space sensor networks for its good character of the traditional tracking methods inadequate. For the localization algorithm and route planning of space sensor network exists a big positioning error in high altitude platform station (HAPS) space communication. Space sensor network communication system is researched. According to the anchor nodes and unknown nodes, location algorithm and node route planning method of HAPS are proposed in this paper. The performance of the node density and location error are simulated and analyzed in HAPS. The simulation results show that the performance of proposed location error is better than the traditional algorithms.

Keywords: Network Communication; Location Algorithm; Anchor Node; Mathematical Model

1 Introduction

The high altitude platform stations (HAPS) is a new information system that has been developed at an early stage in recent years. Stratospheric HAPS is a key instrumentality for broadband wireless communication, as it could complement and cooperate with satellite and terrestrial communications. So far, in the process of studying and developing of space sensor networks, security has been concentrated less. As a new network, the space sensor network is a multi-discipline, highly intersecting researched hot field, which is of both military and business values. Topology control is one of the most fundamental problems in space sensor networks [1-3], which are the newest technology of information collecting and processing, have a wide range of application including military and business. But the node localization information played a key role in the application of space sensor network. The uplink capacity formula for the HAPS-terrestrial CDMA system is deduced and the capacity of the ring structure and that of the multi-layer structure are compared [4-5]. Research of the space sensor network gradually gets the focus from the industrial and academe [6-7]. It has a great application future in the military and civil area. Reducing power consumption to extend network lifetime is one of the most important challenges in designing space sensor networks.

Anchor node positioning usually depends on manual deployment or using GPS. The manual deployment of anchor nodes is not only limited by the network deployment environment. It also severely restricts the

scalability of networks and applications. With GPS positioning. The cost of anchor nodes will be two orders of magnitude higher than that of ordinary nodes. This means that even if only 10% of the nodes are anchor nodes, the price of the entire network will increase by 10 times. In addition, the range of positioning accuracy increases with the increase of the density of anchor nodes. When it reaches a certain level, it will not increase again. Therefore, the density of anchor nodes is also one of the important indicators for evaluating the performance of positioning systems and algorithms.

References [8-15] prolonged network lifetime, good scalability and proper load balancing are important requirements for many sensor network applications. Clustering sensor nodes is an effective technique for achieving these goals. Clustering Algorithm based on Node Correlation (CANC) is proposed. CANC utilizes received signal strength, residual energy and connectivity to choose cluster-heads. It takes the node correlation into account to determine cluster members. Analysis and simulation results show preliminarily that, the new CANC algorithm can make cluster-heads well distributed and achieve good performance in terms of system lifetime, scalability and LBF (load balancing factor). Classic clustering algorithms in space sensor networks are studied and find two main reasons causing unnecessary energy consumption, which are fixed operation periods and too much information exchanged in cluster-heads selection. Then an Energy-Efficient Clustering Algorithm (EECA) is proposed, whose kernels are adaptive operation period model and a new cluster-heads selection method [16-18]. Simulation results show that the proposed protocol can adjust operation period adaptively and reduce the information exchanging in choosing cluster-heads, is more energy-efficient and suitable for space sensor network.

A new location algorithm and route planning for use in space sensor network are studied in References [19-20]. References [21-22] presents the analytic and simulation results of the performance of UWB relative location estimation in space sensor networks, and analyze and evaluate the energy consumption models in space sensor networks with probabilistic distance distributions. References [23-24] propose resolving schemes of data collection in space sensor networks of both plane model and linear and nonlinear mathematics model, and proposed a new node route planning method.

The rest of this paper is organized as follows. In Section II, the space sensor network system of HAPS model node route planning is researched. In Section III, the location algorithm and route planning is built up for the space sensor network communication system. In Section IV, simulation results are presented. Finally, conclusions are drawn in Section V.

2 Node Route Planning

The space sensor network is drawn in Figure.1. Space sensor network includes a anchor nodes and unknown nodes. It can be implemented with a laser or microwave communication between them. It is a challenging problem about the location algorithm. The traditional location algorithm of SCAN [25] for space sensor network can be seen in Fig.1.

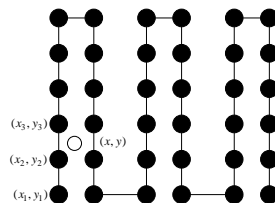


Figure 1. SCAN location algorithm

As can be seen from Fig.1. First, in one direction (such as scanning from outside to inside), the sequence of the requested service is sequentially accessed during the scanning. Scan backwards when scanning to the innermost service sequence. Note here that assuming the innermost layer is track 0. The sequence of the innermost request service is no. 5. After visiting no. 5, it is reversed, and there is no need to sweep back. In the better understanding of the elevator process, when the elevator accesses people, it is clear that the lowest level is no one. It will not go any further. We suppose some node that is the beacon node, the position is (x_1, y_1) , one node is the unknown node, the position is (x, y) , We suppose the distance from the beacon node to unknown node is d_1 , so we can get:

$$(x_1 - x)^2 + (y_1 - y)^2 = d_1^2 \quad (1)$$

$$s.t. \quad 0 \leq x \leq l_1, 0 < y \leq l_2 \quad (2)$$

The traditional location algorithm of CIRCLES for space sensor network [20-21] is shown in Fig.2.

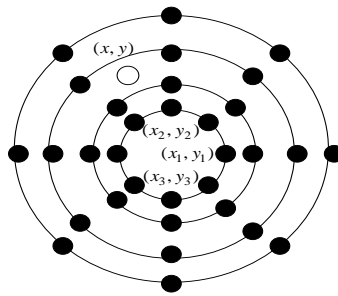


Figure 2. CIRCLES location algorithm

The relationship of multilateral localization of the unknown node is shown in Fig.3.

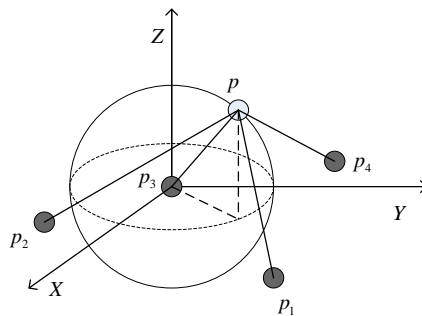


Figure 3. Multilateral localization of the unknown node

There are two beacon nodes in the space sensor network system. The position of beacon node C (x_2, y_2, z_2) , $AC = d_2$, the mathematics model can be denoted as

$$\begin{cases} (x_1 - x)^2 + (y_1 - y)^2 + (z_1 - z)^2 = d_1^2 \\ (x_2 - x)^2 + (y_2 - y)^2 + (z_2 - z)^2 = d_2^2 \\ y = 0 \text{ or } y = l_1 \text{ or } z = l_2 \\ \text{s.t. } 0 \leq y \leq l_1, 0 < z \leq l_2 \end{cases} \quad (3)$$

There are three beacon nodes in the space sensor network system, the mathematics model can be expressed as

$$\begin{cases} (x_1 - x)^2 + (y_1 - y)^2 + (z_1 - z)^2 = d_1^2 \\ (x_2 - x)^2 + (y_2 - y)^2 + (z_2 - z)^2 = d_2^2 \\ (x_3 - x)^2 + (y_3 - y)^2 + (z_3 - z)^2 = d_3^2 \\ y = 0 \text{ or } y = l_1 \text{ or } z = l_2 \\ \text{s.t. } 0 \leq y \leq l_1, 0 < z \leq l_2 \end{cases} \quad (4)$$

The distance of anchor nodes can be calculated as follows:

$$d_{kj} = \begin{cases} [\sum_{i=1}^{l_k} (s_{ki} - x_{ji})^\alpha]^{1/\alpha} & k = 1 \\ [\sum_{i=1}^{l_k} (s_{ki} - x_{j(i+l_{k-1})})^\alpha]^{1/\alpha} & k > 1 \end{cases} \quad k = 1, 2, \dots, M; j = 1, 2. \quad (5)$$

3 Location and Route Planning Algorithm

For space sensor network node location, due to the location of the mobile node insert uncertain nodes, so the inserted into the virtual anchor nodes, which helps to limit the location error. The node system model is shown in Fig.4.

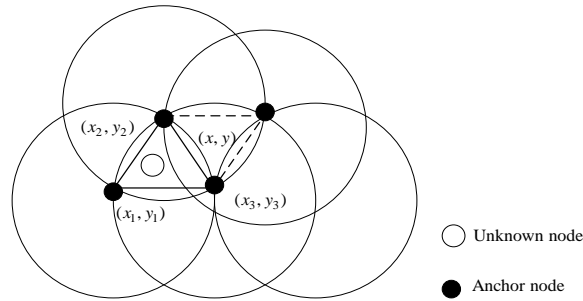


Figure 4. The node system model

The node movement route plan is obtained. So we can get:

$$\begin{cases} x = x_0 + r \times t \times \cos(2\pi t + \varphi) \\ y = y_0 + r \times t \times \sin(2\pi t + \varphi) \end{cases} \quad (6)$$

Similarly, in the triangle, we can get:

$$\cos \theta = \frac{(d_2^2 / 4) + d_1^2 - d_0^2}{d_1 d_2} \quad (7)$$

Combined with formula (6) and (7), d_0 can be expressed as:

$$d_0 = \frac{\sqrt{2d_1^2 + 2d_3^2 - d_2^2}}{2} \quad (8)$$

The total path length can be expressed as

$$D = \sum_{t=1}^{20} \sqrt{r^2 + 4r^2\pi^2t^2 + 4r^2t \sin(4\pi t) + 4r^2t \cos(4\pi t)} \quad (9)$$

The flow chart of space sensor network node location is shown in Fig.5.

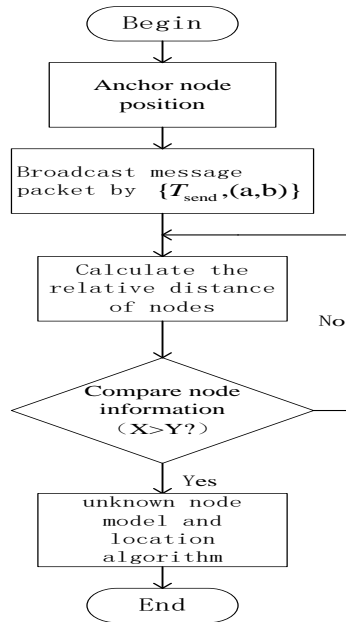


Figure 5. The flow chart of location

Where, the anchor node broadcast message is shown in Fig.6.

We assume that the received packet position is triangle.

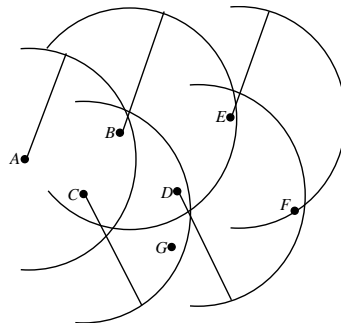


Figure 6. The anchor node of broadcast message

Node relative positioning and the radial error can be expressed respectively:

$$error_{avg} = \frac{\sum_{i=1}^n \sqrt{(x_i - x'_i)^2 + (y_i - y'_i)^2 + (z_i - z'_i)^2}}{n \times R} \times 100\% \quad (10)$$

$$error_x = \frac{\sum_{i=1}^n abs(x_i - x'_i)}{n \times R} \times 100\% \tag{11}$$

4 Simulation Analysis

Considering the 150 nodes to be mounted on the random uniform topology. The relation between node radius and location error is shown in Fig.7.

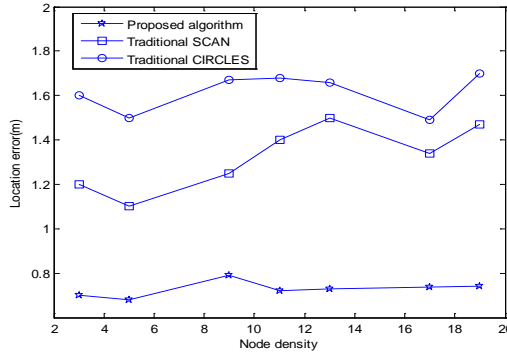


Figure 7. Relation between node density and location error

As can be seen from Fig.7. The location error performance of proposed space sensor network node location algorithm is better than traditional SCAN and CIRCLES. The relation between node density and location proportion is shown in Fig.8.

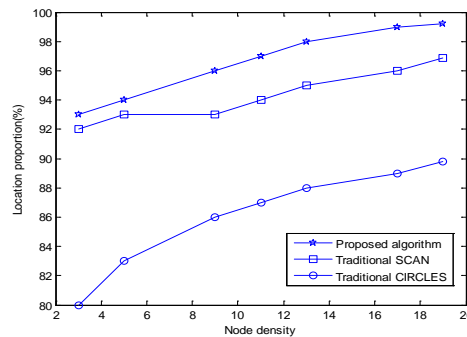


Figure 8. Relation between node density and location proportion

As can be seen from Fig.8. The location proportion performance of proposed space sensor network node location algorithm is better than traditional SCAN and CIRCLES methods. The relation of movement speed of nodes and location error is shown in Fig.9.

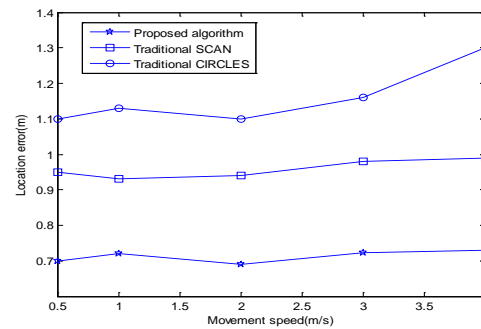


Figure 9. Relation of movement speed and location error

As can be seen from Fig.9. With the increase of movement speed of nodes, the shows different changing tendency along with different location error. In all, the proposed algorithm is better than the traditional SCAN and CIRCLES methods. Location time under different movement speed is shown in Fig.10.

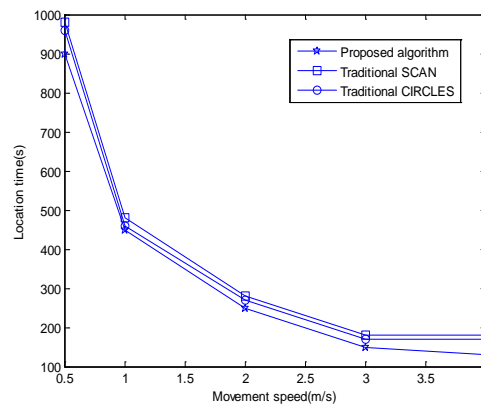


Figure 10. Node density and location error

As can be seen from Fig.10, the location time is different when the movement speed is different. With the increase of movement speed, the location time is becoming less.

5 Summary

Based on the analysis of the space sensor network, some conclusions are obtained. First of all, the space sensor network communication system is set up. Then, location algorithm and node route planning of space sensor network are proposed. Some mathematics model is built according to the space sensor network communication system. Lastly, mathematics model and location algorithm and route planning method are simulated. The performance of the proposed location algorithm and route planning method is better than the traditional methods.

ACKNOWLEDGMENT

The paper was supported by Science and Technology Research Program of Chongqing Municipal Education Commission(KJ1600923,KJ1709206),Young Fund Project of Humanities and Social Sciences Research of Ministry of Education of China (16YJC860010, 15YJC790061,16JDSZ2019),Natural Science Foundation of

China (61571069,61501065,61502064,61503052),Social Science of Humanity of Chongqing Municipal Education Commission(17SKG144),National Social Science Fund of China West Project(17XXW004).2018 Chongqing Science and Technology Commission Technology Innovation and Application Demonstration (Social Livelihood General) Project(cstc2018jscx-msyb0364).The author Xiaoyang Liu thanks for the financial support from CSC (China Scholarship Council)(201608505142).

REFERENCES

- [1]. Marcus.L.Braga,Alyson.J.Santos,“Anytime route planning with constrained devices,”Computers & Electrical Engineering, vol.54, pp.53-67,2016.
- [2]. Jian An,Ling Qi, Xiaolin Gui,Zhenlong Peng,“Joint design of hierarchical topology control and routing design for heterogeneous wireless sensor networks,”Computer Standards & Interfaces, vol.51, pp.63-70,2017.
- [3]. A.Xenakis,F. Foukalas,G.Stamoulis,“Cross-layer energy-aware topology control through Simulated Annealing for WSNs,”Computers & Electrical Engineering, vol.56, pp.576-590,2016.
- [4]. Rachid Beghdad,Mohamed Abdenour Hocini,Narimane Cherchour, Mourad Chelik,“PEAS with Location Information for coverage in Wireless Sensor Networks,”Journal of Innovation in Digital Ecosystems,vol.3, no.2,pp.163-171,2017.
- [5]. Dang Thanh Hai,Le Hoang Son,Trong Le Vinh,“Novel fuzzy clustering scheme for 3D wireless sensor networks,”Applied Soft Computing, vol.54,pp.141-149,2017.
- [6]. Amar Kaswan,Kumar Nitesh,Prasanta K. Jana,“Energy efficient path selection for mobile sink and data gathering in wireless sensor networks,”AEU-International Journal of Electronics and Communications,vol.73,pp. 110-118,2017.
- [7]. Reem E.Mohemed,Ahmed I. Saleh, Maher Abdelrazzak, Ahmed S. Samra,“Energy-efficient routing protocols for solving energy hole problem in wireless sensor networks,”Computer Networks, vol.114,pp. 51-66,2017.
- [8]. Amit Sarkar, T. Senthil Murugan ,“Routing protocols for wireless sensor networks,”Alexandria Engineering Journal,vol.55,no.4, pp.3173-3183, 2016.
- [9]. Guangqiang Chen,Bingyan Chen,Pengfei Li, Peng Bai, Chunqun Ji,“Study of aerodynamic configuration design and wind tunnel test for solar powered buoyancy-lifting vehicle in the near-space,”Procedia Engineering,vol.99,pp.67-72,2015.
- [10]. Guanhua Wang,Shanfeng Zhang,Kaishun Wu,et al,“TIM: fine-grained rate adaptation in wLANs,”IEEE Transactions on Mobile Computing,vol.15,no.3,pp. 748-761,2015.
- [11]. Jie Hu,Lie-Liang Yang,Lajos Hanzo,“Distributed Multistage cooperative-social-multicast-aided content dissemination in random mobile networks,”IEEE Transactions on Vehicular Technology, vol.64, no.7,pp.3075-3089, 2015.
- [12]. Muhammad Aslam,Ehsan Ullah Munir,M. Mustafa Rafique, Xiaopeng Hu,“Adaptive energy-efficient clustering path planning routing protocols for heterogeneous wireless sensor networks,”Sustainable Computing: Informatics and Systems, vol.12, pp.57-71,2016.

- [13]. Yatish K.Joshi, Mohamed Younis, "Restoring connectivity in a resource constrained WSN," *Journal of Network and Computer Applications*, vol. 66, pp.151-165,2016.
- [14]. Bibin Varghese, Nidhin Easow John, S. Sreelal, Karthika Gopal, "Design and Development of an RF Energy Harvesting Wireless Sensor Node (EH-WSN) for Aerospace Applications," *Procedia Computer Science*, vol.93, pp.230-237,2016.
- [15]. Nouha Baccour, Anis Koubaa, Habib Youssef, Mario Alves, "Reliable link quality estimation in low-power wireless networks and its impact on tree-routing," *Ad Hoc Networks*, vol.27, pp.1-25,2015.
- [16]. Juan J. Galvez, Pedro M. Ruiz, "Joint link rate allocation, routing and channel assignment in multi-rate multi-channel wireless networks," *Ad Hoc Networks*, vol.29, pp.78-98,2015.
- [17]. Ajinkya Rajandekar; Biplab Sikdar, "A survey of MAC layer issues and protocols for machine-to-machine communications," *IEEE Internet of Things Journal*, vol.2, no.2, pp.175-186, 2015.
- [18]. Rodolfo Feick, Mauricio Rodríguez, Luciano Ahumada, et al, "Achievable gains of directional antennas in outdoor-indoor propagation environments," *IEEE Transactions on Wireless Communications*, vol.14, no.3, pp.1447-1456,2015.
- [19]. Prasenjit Chanak, Indrajit Banerjee, R. Simon Sherratt, "Energy-aware distributed routing algorithm to tolerate network failure in wireless sensor networks," *Ad Hoc Networks*, vol.56, no.1, pp.158-172,2017.
- [20]. Felipe Núñez, Yongqiang Wang, David Grasing, "Pulse-coupled time synchronization for distributed acoustic event detection using wireless sensor networks," *Control Engineering Practice*, vol.60, pp.106-117,2017.
- [21]. Kejiang Xiao, Rui Wang, Tun Fu, Jian Li, Pengcheng Deng, "Divide-and-conquer architecture based collaborative sensing for target monitoring in wireless sensor networks," *Information Fusion*, vol.36, pp.162-171,2017.
- [22]. Mohammad Shokouhifar, Ali Jalali, "Optimized sugeno fuzzy clustering algorithm for wireless sensor networks," *Engineering Applications of Artificial Intelligence*, vol.60, pp.16-25,2017.
- [23]. Zhibo Wang, Honglong Chen, Qing Cao, Hairong Qi, Zhi Wang, Qian Wang, "Achieving location error tolerant barrier coverage for wireless sensor networks," *Computer Networks*, vol.112, pp.314-328,2017.
- [24]. Demin Gao, Haifeng Lin, Xiaofeng Liu, "Routing protocol for k-anycast communication in rechargeable wireless sensor networks," *Computer Standards & Interfaces*, vol.43, pp.12-20, 2016.
- [25]. Reem E. Mohamed, Ahmed I. Saleh, Maher Abdelrazzak, Ahmed S. Samra, "Energy-efficient routing protocols for solving energy hole problem in wireless sensor networks," *Computer Networks*, vol.114, pp.51-66,2017.

Ecological Methods of Assessing the Quality of the Environment in the Fluctuating Asymmetry of Birch Leaves

P.M. Mazurkin

*Dr. Sc., Prof., Volga State University of Technology, Yoshkar-Ola, Russia,
kaf_po@mail.ru*

ABSTRACT

The methods of ecological assessment of the environmental quality of growing birch trees on fluctuating asymmetry of leaves after their stop in growth are briefly presented. In comparison with the average values of parameter measurements, each of the five leaves from at least three birches improves the accuracy of modeling and seven times reduces the complexity of measurements.

Key words: three birches, on five leaves, 10 parameters, factor analysis, correlation coefficient, strong regularities

1 Introduction

In environmental technology is gradually coming to an understanding of the need for modeling relationships between the parameters of structure of plant leaves identification method (Mazurkin, 2014a, b).

Our Russian inventions (Mazurkin, Semenova, 2016a, b, c, d, e, f) refers to the engineering of biology and bioindication of the environment quality measurements of the growth of the organs of different plant species, mostly woody plants, for example, samples in the form of leaves of birch trees with a simple and small leaf blades.

The technical result is an increase in the accuracy of indication of the quality of the surrounding birch leaves of the local environment, as well as simplifying and improving the performance of measurements of leaf parameters. Thus, we completely restore the principle of individuality of biological measurements on the geometry of fluctuation of each sheet.

2 The Method of Measurement and Analysis

Figure 1 shows a diagram of the dimensions of each sheet: 1 - the width of the left b' and right b'' halves of the leaf (the measurement was carried out in the middle of the leaf blade), mm; 2 - length l'_{oc} and l''_{oc} the second from the base of the leaf veins of the second order, mm; 3 – distance l'_{och} and l''_{och} between the bases of the first and second veins of second order, mm; 4 – distance l'_κ and l''_κ between the ends of these veins, mm; 5 – angle α' and α'' between the main vein and the second from the base of the leaf vein of the second order. Collection of material should be carried out after stopping the growth of leaves (in the middle lane since July).

For environmental assessment of anthropogenic impact on the territory take at least three birches in approximately the same conditions of growth, with each birch take at least five leaves of different sizes on the part of the estimated area, then the measurement of the five parameters of the sheet is carried out with the use of geodetic protractor with the price of dividing the measuring scale of 0.1 mm, with all at least 15 leaves are taken for the population of individual individuals, therefore, the table of measurement results without averaging the measured values is further compiled, and the resulting sample is statistically simulated and subjected to factor analysis to identify binary relations between 10 indicators, with all 100 biotechnical laws identified in the software environment CurveExpert-1.40 by the formula of the form

$$y = a_1 x^{a_2} \exp(-a_3 x^{a_4}) + a_5 x^{a_6} \exp(-a_7 x^{a_8}) \quad (1)$$

where y - an indicator or a dependent quantitative factor (10 parameters for five indicators from two halves of the sheet); x - an explanatory variable or an influencing factor (the same 10 parameters from each sheet); $a_1 \dots a_8$ - the model parameters obtained by identification.

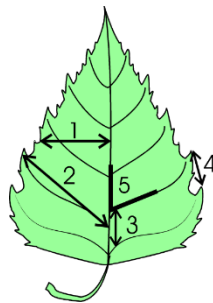


Figure 1

Corresponding Author: Peter Mathveevich Mazurkin, Volga State University of Technology, 424000, the Republic of Mari El, Yoshkar-Ola, Lenin Sq., b. 3, Email: kaf_po@mail.ru

According to the results of factor analysis by identifying binary relations between 10 indicators perform environmental assessment of the territory by the coefficient of correlation variation, and then from 100 biotechnical laws are selected having a correlation coefficient of at least 0,7 and consider pairwise five parameters of the sheet, as well as environmental assessment is carried out by differences between the structure and parameters of specific equations.

The results of the measurements in a clean area of the city of Zvenigovo Republic of Mari El

According to the principle of individuality of each leaf, the results of measuring the parameters of 15 leaves of only three birches in a clean area are listed in table 1.

**Table 1. Results of measurements of birch leaves growing in the clean zone of the city
(on 5 of leaves with 3 plants)**

№ trees	№ sheet	Width b , mm		Length, $l_{\text{жс}}$, mm		Distance $l_{\text{оч}}$, mm		Distance $l_{\text{к}}$, mm		Corner α , degree	
		left b'	right b''	left $l'_{\text{жс}}$	right $l''_{\text{жс}}$	left $l'_{\text{оч}}$	right $l''_{\text{оч}}$	left $l'_{\text{к}}$	right $l''_{\text{к}}$	left α'	right α''
1	1	18	17	32	30	8	8	10	10	30	28
	2	19	21	33	36	9	8	12	13	34	39
	3	22	19	36	32	6	8	14	14	37	33
	4	17	20	31	31	5	7	13	11	44	34
	5	16	17	29	31	12	11	12	16	30	31
2	6	16	17	28	29	5	6	10	10	34	37
	7	17	15	31	29	3	2	10	9	43	37
	8	18	18	33	32	5	5	11	9	37	36
	9	16	19	28	32	5	5	10	11	38	42
	10	23	21	37	40	5	6	12	13	38	37
3	11	18	19	31	33	5	4	13	12	49	49
	12	17	16	30	30	5	4	10	11	46	43
	13	23	21	40	40	4	3	15	15	48	42
	14	16	20	37	35	6	8	13	12	44	44
	15	23	22	37	40	6	7	14	15	46	44

Full factorial analysis includes 10 factors and $102 = 100$ factor relations. For all of them the equation has the form of (1).

The correlation matrix of the factor analysis for assessment of a condition of the environment is given in table 2.

Table 2. Correlation matrix of the full factorial analysis of plastic signs of leaves of a birch for assessment of a condition of the environment

The influencing factors x	Dependent factors (indicators y)										Sum $\sum r_x$	Place I_x
	b'	b''	$l'_{\text{жс}}$	$l''_{\text{жс}}$	$l'_{\text{оч}}$	$l''_{\text{оч}}$	$l'_{\text{к}}$	$l''_{\text{к}}$	α'	α''		
Width b' , mm	1	0,6530	0,8105	0,8210	0,1700	0,0905	0,6621	0,6639	0,2740	0,1222	5,2672	6
Width b'' , mm	0,7179	1	0,7139	0,9185	0,2413	0,4052	0,7404	0,5721	0,4132	0,3913	6,1138	2
Length $l'_{\text{жс}}$, mm	0,8058	0,6806	1	0,8340	0,2299	0,1746	0,7572	0,5652	0,4036	0,2785	5,7294	5
Length $l''_{\text{жс}}$, mm	0,8175	0,9144	0,8133	1	0,3181	0,3546	0,7190	0,6315	0,3420	0,4419	6,3523	1
Distance $l'_{\text{оч}}$, mm	0,2712	0,4867	0,3173	0,2346	1	0,8960	0,1701	0,4796	0,6639	0,4962	5,0156	8
Distance $l''_{\text{оч}}$, mm	0,2776	0,4977	0,0818	0,2226	0,9262	1	0,2068	0,5337	0,6369	0,5953	4,9786	9
Distance $l'_{\text{к}}$, mm	0,5290	0,7585	0,7693	0,6791	0,4647	0,3308	1	0,7367	0,5290	0,2888	6,0859	3
Distance $l''_{\text{к}}$, mm	0,5851	0,7079	0,4921	0,6560	0,5585	0,4618	0,7553	1	0,2643	0,4204	5,9014	4
Corner α' , degree	0,2573	0,3117	0,3686	0,3450	0,7079	0,6413	0,4834	0,1871	1	0,7796	5,0819	7
Corner α'' , degree	0,1405	0,3644	0,2091	0,4233	0,4177	0,5406	0,2787	0,1283	0,7796	1	4,2822	10
Sum $\sum r_y$	5,4019	6,3749	5,5759	6,1341	5,0343	4,8954	5,773	5,4981	5,3065	4,8142	54,8083	-
Place I_y	6	1	4	2	8	9	3	5	7	10	-	0,5480

The coefficient of correlation variation of the ecological set of 15 leaves (5 leaves from 3 trees) is $54,8083 / 10^2 = 0,5480$. This criterion is used when comparing different sampling sites of birch leaves. In comparison with table 2, variability in fluctuating asymmetry increased significantly, as 0.5480.

3 Analysis of Binary Relations between Factors

To do this, we exclude monary relations from the data 1, we leave only binary relations with strong factorial relations (table. 3). There are 22 strong binary dependencies left. The formula $l''_{och} \rightarrow l'_{och}$ has the highest strength. The distance between the bases of the first and second veins on the right side of the leaves most affects the distance between the bases of the first and second veins on the left side of the leaves.

Table 3. Correlation matrix of strong binary relations of plastic signs of birch leaves under condition $r \geq 0,7$

The influencing factors x	Dependent factors (indicators y)									
	b'	b''	$l'_{\text{жс}}$	$l''_{\text{жс}}$	$l'_{\text{оч}}$	$l''_{\text{оч}}$	$l'_{\text{к}}$	$l''_{\text{к}}$	α'	α''
Width b' , mm			0,8105	0,8210						
Width b'' , mm	0,7179		0,7139	0,9185			0,7404			
Length $l'_{\text{жс}}$, mm	0,8058			0,8340						
Length $l''_{\text{жс}}$, mm	0,8175	0,9144	0,8133				0,7190			
Distance $l'_{\text{оч}}$, mm						0,8960				
Distance $l''_{\text{оч}}$, mm					0,9262					
Distance $l'_{\text{к}}$, mm		0,7585	0,7693					0,7367		
Distance $l''_{\text{к}}$, mm		0,7079					0,7553			
Corner α' , degree					0,7079					0,7796
Corner α'' , degree									0,7796	

For example, figure 2 shows a graph of the effect of $l''_{och} \rightarrow l'_{och}$ the distance between the bases of the first and second veins on the right side of the leaves by the distance between the bases of the first and second veins on the left side of the leaves when measured by the proposed method on 15 leaves in three birches. Figure 3 shows a graph of the result $b'' \rightarrow l''_{\text{жс}}$ of the influence of the width on the right side of the leaves on the length of the second vein on the right side of the leaves.

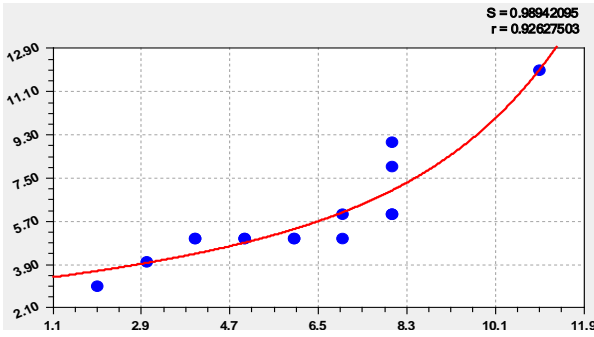


Figure 2. Graph of the formula $l''_{OCH} \rightarrow l'_{OCH}$

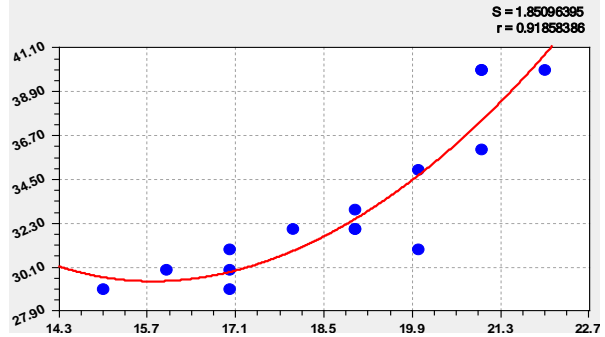


Figure 3. Graph of the formula $b'' \rightarrow l''_{ЖC}$

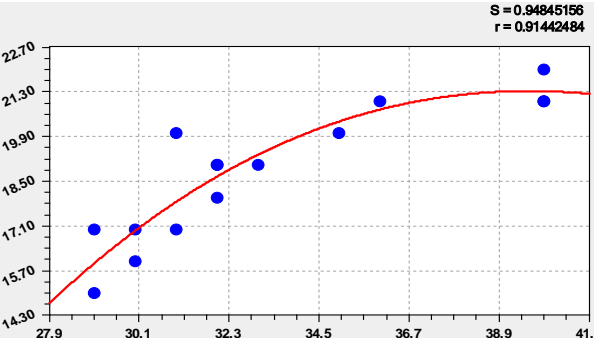


Figure 4. Graph of the formula $l''_{ЖC} \rightarrow b''$

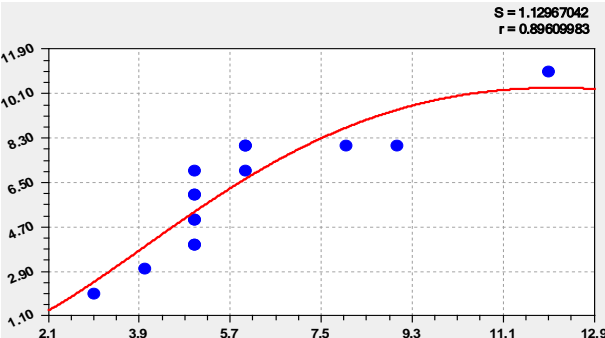


Figure 5. Graph of the formula $l'_{OCH} \rightarrow l''_{OCH}$

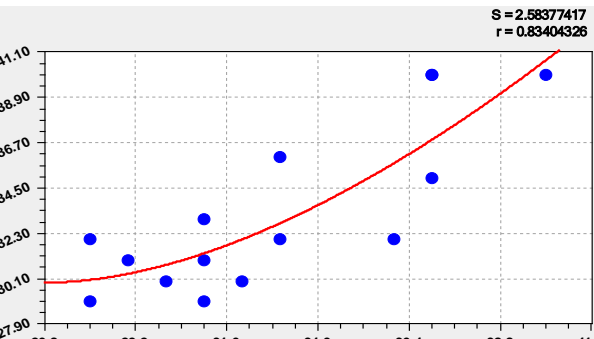


Figure 6. Graph of the formula $l'_{ЖC} \rightarrow l''_{ЖC}$

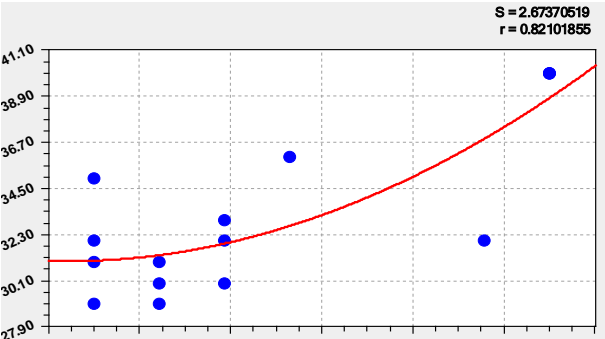


Figure 7. Graph of the formula $b' \rightarrow l''_{ЖC}$

On figure 4 - graph of the result $l''_{ЖC} \rightarrow b''$ influence of the length of the second vein on the right side of the leaves on the width on the right side of the leaves. On a figure 5 shows the graph of the result $l'_{OCH} \rightarrow l''_{OCH}$ of the influence of the distance between the bases of the first and second veins on the left side of the leaves on the distance between the bases of the first and second veins on the right side of the leaves. On a figure 6 - graph of the result $l'_{ЖC} \rightarrow l''_{ЖC}$ influence of the length of the second vein on the left side of the leaves on the length of the second vein on the right side of the leaves. On a figure 7 shows the graph of $b' \rightarrow l''_{ЖC}$ effect of width on the left side of leaves on the length of the second vein on the right side of leaves

4 Comparison of the Proposed Methods with the Prototype

Thus, the comparison shows that the proposed information technology for processing the values of the same parameters in individual leaves $57 / 22 = 2,59$ times stricter than the prototype.

The correlation coefficient is also $0,7538 / 0,5480 = 1,38$ times less, which indicates better variability. Therefore, it can be concluded that the adoption of the arithmetic mean values of the parameters of birch leaves up to 100 (10 trees for 10 leaves) is artificial, smoothing the variability of fluctuating asymmetry. In reality, it is much more variable.

All 22 strong links in table 3 are arranged without the loss of a row and form a geometric pattern. This fact also points to the application of the principle of individuality, that is, without averaging the results of environmental measurements.

Write out the formula 22 binary factor strong ties, ranging in table 4 in descending order of correlation coefficient.

Table 4. Options patterns binary strong ties factors

№ π/π	$x \rightarrow y$	$y = a_1 x^{a_2} \exp(-a_3 x^{a_4}) + a_5 x^{a_6} \exp(-a_7 x^{a_8})$								Correlation coefficient r
		The first component				Second component				
		a_1	a_2	a_3	a_4	a_5	a_6	a_7	a_8	
1	$l''_{оч} \rightarrow l'_{оч}$	3,071555	0	0,071176	1	0,037407	0,39827	0,36397	1	0,9262
2	$b'' \rightarrow l''_{жс}$	216,90035	0	0,18129	1	0,48931	0,82839	0,079967	1	0,9185
3	$l''_{жс} \rightarrow b''$	0,13005	2,26719	0,057208	1	35,24084	0	0	1	0,9144
4	$l'_{оч} \rightarrow l''_{оч}$	0,37763	2,21272	0,18243	1	0	0	0	1	0,8960
5	$l'_{жс} \rightarrow l''_{жс}$	285,55703	0	0,13188	1	0,61588	0,94539	0,016692	1	0,8340
6	$b' \rightarrow l''_{жс}$	83,922	0	0,10854	1	0,62999	0,88169	0,050474	1	0,8210
7	$l''_{жс} \rightarrow b'$	429,19236	0	0,15290	1	0,25493	0,89348	0,028748	1	0,8175
8	$l''_{жс} \rightarrow l'_{жс}$	9,96212	0	0,019433	1	0,74876	1,025059	0,00041489	1	0,8133
9	$b' \rightarrow l'_{жс}$	45,87364	0	0,081235	1	0,85588	0,92382	0,029908	1	0,8105
10	$l'_{жс} \rightarrow b'$	0,0097932	2,10278	0,0099842	1	7,62307	0	0	1	0,8058
11	$\alpha' \rightarrow \alpha''$	5,52381	0	0,0057460	1	2,68220	0,62964	0,0054722	1	0,7796
12	$\alpha'' \rightarrow \alpha'$	1,99219	0	0,039772	1	1,065425	1,035282	0,010853	1	0,7796
13	$l'_{к} \rightarrow l'_{жс}$	33,97637	0	0,041107	1	0,39111	0,61879	0,15405	1	0,7693
14	$l'_{к} \rightarrow b''$	0,098318	3,010187	0,19554	1	2,58419	0	0	1	0,7585
15	$l''_{к} \rightarrow l'_{к}$	0,017059	3036064	0,19256	1	4,97922	0	0	1	0,7553
16	$b'' \rightarrow l'_{к}$	110,10051	0	0,40834	1	0,60848	1,01504	0,00041684	1	0,7404
17	$l'_{к} \rightarrow l''_{к}$	4,27876	0,78319	0,023133	1	10,46382	0	0	1	0,7367
18	$l''_{жс} \rightarrow l'_{к}$	0,087963	2,27808	0,058024	1	25,015367	0	0	1	0,7190
19	$b'' \rightarrow b'$	125,22754	0	0,16146	1	0,13403	0,73296	0,12324	1	0,7179
20	$b'' \rightarrow l'_{жс}$	138,011555	0	0,16128	1	0,75209	0,91987	0,043949	1	0,7139
21	$l''_{к} \rightarrow b''$	0,14397	3,050669	0,22213	1	0	0	0	1	0,7079
22	$\alpha' \rightarrow l'_{оч}$	33,68506	0	0,044599	1	0	0	0	1	0,7079

Matrix representation of the model (1) is compact, but for clarity we will write the first three binary relationships separately in the form of formulas:

- effect of the distance between the bases of the first and second veins on the right side of the leaves on the distance between the bases of the first and second veins (Figure 2) on the left side of the leaves

$$l'_{och} = 3,071555 \exp(0,071176 l''_{och}) + 0,037407 l''_{och}{}^{0,39827} \exp(0,39827 l''_{och}); \quad (2)$$

- effect of width on the right side of the leaves on the length of the second vein (Figure 3) on the right side of the leaves

$$l''_{oc} = 216,90035 \exp(0,18129 b'') + 0,48931 b''^{0,82839} \exp(0,079967 b''); \quad (3)$$

- the effect of the length of the second vein on the right side of the leaves on the width on the right (Figure. 4) side of the leaves

$$b'' = 0,13005 l''_{oc}{}^{2,26719} \exp(-0,057208 l''_{oc}) - 35,24084 \quad (4)$$

5 Conclusion

Thus, fluctuating asymmetry can be captured by statistical modelling from a much smaller volume of measurements. The smallest volume of measurements we recommend 15 (three trees of five different leaf sizes from different places). This will reduce the volume of measurements $100 / 15 \approx 7$ times. However, this increases the accuracy of the analysis of fluctuating asymmetry.

The advantage of the proposed method is the technical simplicity of execution, since the equipment requires only a measuring pair of compasses and surveying protractor with scale division 0,1 mm. Therefore, the invention can be widely implemented in school environmental clubs, school forestries, and even kindergartens, as well as in geographical and other expeditions with additional study of the quality of the territory on the properties of the leaves of the birch trees.

REFERENCES

- [1] Mazurkin, P.M. Method of identification. (2014). International Multidisciplinary Scientific GeoConference Surveying Geology and Mining Ecology Management, SGEM, 1 (6), pp. 427-434. <https://www.scopus.com/inward/record.uri?eid=2-s2.0-84946541076&partnerID=40&md5=72a3fccc31b20f2e63e4f23e9a8a40e3>
- [2] Mazurkin, P.M. Identification of the wave patterns of behavior. (2014). International Multidisciplinary Scientific GeoConference Surveying Geology and Mining Ecology Management, SGEM, 1 (6), pp. 373-380. <https://www.scopus.com/inward/record.uri?eid=2-s2.0-84946550468&partnerID=40&md5=0fd8f91ed5b1f0592fc587e5ffb14e51>
- [3] Patent 2549779 Russian Federation, IPC A 01 G 23 / 00 (2006.01). The way the environmental dimension of the sides of the birch of the municipal Park in the fluctuating asymmetry of leaves / Mazurkin, P.M., Semenov D.V.; applicant and patentee Volga state University of technology No. 2013136883/13; stated 06.08.2013; published 27.04.2015. Bulletin No. 12. <http://www1.fips.ru/Archive/PAT/2015FULL/2015.04.27/DOC/RUNWC2/000/000/002/549/779/document.pdf>
- [4] Patent 2556980 Russian Federation, IPC A 01 G 23 / 00 (2006.01). Method of ecological measurement of birch bark on fluctuating asymmetry of leaves / Mazurkin, P.M., Semenova D.V.; applicant and patentee Volga state

technological University №2013136716/13; announced 06.08.2013; published 20.07.2015. Bulletin No. 20. <http://www1.fips.ru/Archive/PAT/2015FULL/2015.07.20/DOC/RUNWC2/000/000/002/556/980/document.pdf>

- [5] Patent 2556985 Russian Federation, IPC A 01 G 23 / 00 (2006.01). Method of comparative indication on fluctuating asymmetry of birch leaves / Mazurkin, P.M., Semenova D.V.; applicant and patentee Volga state technological University №2013136813/13; announced 06.08.2013; published 20.07.2015. Bulletin No. 20. <http://www1.fips.ru/Archive/PAT/2015FULL/2015.07.20/DOC/RUNWC2/000/000/002/556/985/document.pdf>
- [6] Patent 2556987 Russian Federation, IPC A 01 G 23 / 00, A 01 G 7/00 (2006.01). The method of measuring fluctuating asymmetry of birch leaves / Mazurkin, P. M., Semenov D. V.; applicant and patentee Volga state University of technology No. 2013130471/13; stated 02.07.2013; published 20.07.2015. Bulletin No. 20. <http://www1.fips.ru/Archive/PAT/2015FULL/2015.07.20/DOC/RUNWC2/000/000/002/556/987/document.pdf>
- [7] Patent 2569748 Russian Federation, IPC G 01 N 33 / 46 (2006.01). Method a comparative indication of contamination of the air in the fluctuating asymmetry of birch leaves / Mazurkin, P. M., Semenov D. V.; applicant and patentee Volga state University of technology No. 2013134056/13; stated 19.07.2013; published on 27.11.2015. Bulletin No. 33. <http://www.fips.ru/Archive/PAT/2015FULL/2015.11.27/DOC/RUNWC2/000/000/002/569/748/document.pdf>
- [8] Patent 2580647 Russian Federation, IPC G 01 N 33 / 46 (2006.01). Method of indication of air pollution by fluctuating asymmetry of birch leaves / Mazurkin, P.M., Semenova D.V.; applicant and patentee Volga state technological University №2013136714/15; declared 06.11.2013; published 27.05.2015. Bulletin No. 15. <http://www.fips.ru/Archive4/PAT/2016FULL/2016.04.10/DOC/RUNWC2/000/000/002/580/647/document.pdf>